Visualizing the substrate-, superoxo-, alkylperoxo- and product-bound states at the non-heme Fe(II) site of homogentisate dioxygenase

Jae-Hun Jeoung*, Martin Bommer*,†, Tzong-Yuan Lin*, and Holger Dobbek*,‡

* Institut für Biologie, Strukturbiologie/Biochemie, Humboldt-Universität zu Berlin, Unter den Linden 6, 10099 Berlin, Germany

† Macromolecular Crystallography, Soft Matter and Functional Materials, Helmholtz-Zentrum Berlin für Materialien und Energie, Albert-Einstein-Strasse 15, 12489 Berlin, Germany

‡ To whom correspondence should be addressed. E-mail: holger.dobbek@biologie.hu-berlin.de

Phone: ++49-30-2093-6369; Fax: ++49-30-2093-6447

ABBREVIATIONS

HGDO, homogentisate 1,2-dioxygenase; $HGDO_{Pp}$, HGDO from *Pseudomonas putida*; $HGDO_{Hs}$, HGDO from Human; HG, homogentisate; ITC, isothermal titration calorimetry.

MATERIALS AND METHODS

Materials

Pseudomonas putida KT2440 was obtained from the German Collection of Microorganisms and Cell Cultures GmbH - DSMZ (Braunschweig, Germany). All enzymes used for DNA preparation were purchased from Thermo Scientific (Waltham, MA, USA) except for *Pfu* DNA polymerase, which was obtained from New England Biolabs.

All chromatography columns and materials were obtained from GE Healthcare except for the CHT® ceramic hydroxyapatite (type I, 20 µm) material, which was obtained from Bio-Rad. Homogentisate (HG) was purchased from Fluka. All other chemicals used were of at least analytical grade and obtained from Fluka, Sigma or Merck.

Cloning, expression and purification of the wild type $HGDO_{Pp}$

The gene, *hmgA* encoding homogentisate 1,2-dioxygenase ($HGDO_{Pp}$) was amplified from the genomic DNA of *P. putida* by PCR with *Pfu* DNA polymerase using two primers (Forward_hgdo with sequence of 5´– TACATATGAACCGCGACACGTCGCC –3` and Reverse_hgdo with 5´– CCGGATCCTTATCTCCGGTTCGG –3`, where the restriction sites for the enzymes *Nde*I and *Bam*HI are underlined, respectively). A 1301 bp PCR product was digested with *Nde*I and *Bam*HI and ligated into a *Nde*I/*Bam*HI-digested pET11a vector before transformation of *E. coli* DH5α. A positive clone was confirmed by DNA sequencing of the plasmid (Eurofins MWG Operon, Germany) and was named pPKHmgA.

Plasmid pPKHmgA was transformed into *E. coli* BL21(DE3), which was cultivated in LB media containing carbenicillin at 37 °C. When the culture reached the OD_{600} of 0.7, addition of 0.2 mM IPTG induced expression of $HGDO_{Pp}$. Fermentation was continued at 30 °C for additional 6 hours before the cells were harvested. The cell pellet was kept at –30 °C.

Frozen cell paste was resuspended in 70 mL buffer A (50 mM MOPS pH 6.9 and 1 mM TCEP, tris-2-carboxyethylphosphine). Cells were broken by sonication (Branson sonifier) in a glass rosette on ice. After centrifugation at 36,000 rpm for 1 h, the supernatant was applied to a Source 30Q column (30 mL) equilibrated in buffer A. Protein was eluted with 300 mL of a linear gradient of 0 – 1 M NaCl in buffer A. Fractions containing $HGDO_{Pp}$ were eluted at around 300 mM NaCl and pooled and loaded onto a CHT® ceramic hydroxyapatite (20 mL) column equilibrated with a buffer containing 5 mM KH_2PO_4 pH 6.9 and 1 mM TCEP. A peak containing pure $HGDO_{Pp}$ was collected during washing and concentrated. Buffer was changed to buffer A containing 150 mM NaCl using a PD10 column.

Mutagenesis, expression and purification of mutant Y346F-$HGDO_{Pp}$

Site-directed mutagenesis to create the Y346F and H288Q constructs were carried out by whole plasmid PCR. The wild type plasmid was first amplified with Phusion Polymerase using back-to-

back primers with the mutation encoded in the 5' end of one primer. 100 ng of the resulting product was then treated with T4 polynucleotide kinase and T4 DNA ligase to yield the mutant plasmid, and the mutation was confirmed by DNA sequencing (Eurofins MWG Operon, Germany)
Expression and purification of the Y346F- and H288Q-$HGDO_{Pp}$ variants was achieved as described for the wild-type protein.

Activity assays

$HGDO_{Pp}$ activity measurements were performed spectrophotometrically using an Agilent 8453 photodiode array spectrophotometer at 25 °C. The reaction mixture was prepared in an air-saturated buffer consisting of 50 mM MOPS pH 6.9, 100 mM NaCl and 1 mM TCEP. Concentrations of the wild type and the $HGDO_{Pp}$ variants, Y346F and H288Q, in the assay were 60 nM, 140 nM and 5.9 µM, respectively. The reaction was initiated by adding homogentisate to give a final concentration of 500 µM and accumulation of the product, maleylacetoacetate, was monitored at 318 nm (ε_{318} = 11,900 M^{-1} cm^{-1}) (1). Steady-state kinetic parameters, K_m and V_{max} were determined by varying homogentisate concentrations (0 – 500 µM) in three independent measurements. Data were fitted to the Michaelis-Menten equation using the program GraFit 5 (2). The unit of activity is defined as micromoles of maleylacetoacetate produced per minute.

Modeling and refinement of ligands

All ligand F_{obs} − F_{calc} omit maps were calculated after either removal of the ligand or placement of a control ligand to challenge the proposed model. This was followed by several cycles of refinement to reduce model bias.

The active site of HG-bound $HGDO_{Pp}$ was initially assessed by examining the observed F_{obs} − F_{calc} density in the Fe^{2+} bound structure (Fig. 2), and HG was placed into the observed omit map. Active sites of the Fe^{2+}:HG-O_2 structure were then refined against the Fe^{2+}:HG model lacking Fe^{2+} bound solvent molecules. While in eight chains of the Fe^{2+}:HG-O_2 structure, the electron density confirmed the Fe^{2+}:HG model, clear differences in $2F_{obs} – F_{calc}$ and $F_{obs} – F_{calc}$ maps were observed in the other four chains (chains A, C, F and L). Further adaptations of the model were based on interpretation of the observed F_{obs} − F_{calc} difference maps after refinement against Fe^{2+}:HG (Fig. 3, S3, and S4).

Superoxo:semiquinone intermediate in chain C. Additional strong positive peaks in the F_{obs} − F_{calc} difference map were interpreted as the semiquinone state of HG and a side-on binding of a dioxygen molecule (Figs. S3 and Fig. 3a): Firstly, the appearance of puckered electron density at the C2 atom of HG (deviation of planarity of aromatic ring), possibly resulting from the oxidation of HG by a bound electron acceptor (dioxygen), was satisfied by modeling as HG:semiquinone. Secondly, an elongated positive density observed in the W2 position of Fe^{2+}:HG (Fig. 2) could not be explained by a single water ligand. When modeled as such, the result was additional positive

density at a distance of ~1.3 Å, which is unusually short for two solvent molecules (Fig. S3b). The side-on bound dioxygen model clearly explains the longish positive density (Fig. 3a).

Alkylperoxo intermediate in chain F and L. Additional elongated electron density was discerned at the C2 atom of HG and further towards the Fe^{2+} ion when modeled as Fe^{2+}:HG (Fig. S4a and c). We refined the observed density by modeling as superoxo:semiquinone, and this resulted in an extra positive density above the $O1_{O2}$ atom at the position of O1 in $C2_{HG}$–$O1_{O2}$–$O2_{O2}$ of the final alkylperoxo intermediate model (Fig. S4b and d). Further refinement of the positive density with an alkylperoxo moiety (with an occupancy of ~80 and ~60% for chains F and L respectively) (Tab. S3), eliminated the positive density and fully explained the calculated Fourier maps (Fig. 3b). Modeling as simply another conformation of side-on bound O2 led to a clash between $C2_{HG}$ and $O1_{O2}$ due to a short distance (~1.5 Å), which is better explained by a covalent bond between carbon and oxygen. However, we can not exclude a small subpopulation of other states, such as superoxo:semiquinone.

Reproducibility of the O_2-reacting structure

Several other crystals soaked in air for up to an hour as described in the materials and methods produced diffraction to a lower resolution of 2.5 Å. However, at this resolution clear electron density for either HG or the intermediates reported here was not observed. These structures in general showed relatively diffused electron densities, indicating mixed states of Fe^{2+} only, Fe^{2+} :HG or any of the intermediates. We could thus not assign specific states to specific subunits as shown in Fig. S8 for the 1.7 Å structure discussed. Apart from the difficulty in obtaining highly diffracting crystals, this may be due to the fact that 1) the real substrate, rather than a slow-turning over analogue was used and 2) crystal size could have affected diffusion of oxygen from air through the crystal lattice.

References

1. Amaya AA, Brzezinski KT, Farrington N, & Moran GR (2004) Kinetic analysis of human homogentisate 1,2-dioxygenase. *Arch Biochem Biophys* 421(1):135-142.
2. Leatherbarrow RJ (2001) GraFit Version 5 (Ltd., E. S., ed) (Horley, UK).
3. Weiss MS (2001) Global indicators of X-ray data quality. *J Appl Crystallogr* 34:130-135.
4. Ho BK & Gruswitz F (2008) HOLLOW: generating accurate representations of channel and interior surfaces in molecular structures. *BMC Struct Biol* 8:49.

SUPPORTING TABLES

Table S1. Statistics on diffraction data collections and structure refinements of a resting state (Fe^{2+}-only), a complex of $HGDO_{Pp}$ with homogentisate (Fe^{2+}:HG) and Fe^{2+}:HG complex soaked with dioxygen (Fe^{2+}:HG-O_2)

		Fe^{2+}-only	**Fe^{2+}:HG**		**Fe^{2+}:HG-O_2**	
Data collection						
	Wavelength (Å)	0.9184	0.9184		0.9184	
	Space group	*P*1	*P*1		*P*1	
Cell constants	*a, b, c (Å)*	93.39, 93.71, 162.98	93.74, 93.90, 162.81		93.74, 93.86, 163.44	
	α, β, γ (°)	87.69, 80.42, 68.40	87.46, 80.45, 68.34		87.62, 80.39, 68.29	
	Total / unique refl.	1 037 653 / 351 613	987 182 / 337 386		1 527 795 / 532 721	
	R_s [a]	9.0 (45.0)	10.2 (59.0)		8.2 (53.9)	
	$R_{r.i.m.}$ [b]	11.2 (49.2)	12.9 (65.8)		10.3 (60.7)	
	$R_{p.i.m.}$ [b]	6.4 (28.6)	7.4 (37.4)		6.0 (35.5)	
	Resolution (Å)	35 – 1.95 (2.00 – 1.95)	35 – 1.98 (2.03 – 1.98)		35 – 1.70 (1.74 – 1.70)	
	Completeness (%)	94.8 (80.0)	95.6 (91.5)		94.9 (91.1)	
	(I) / (σI)	10.6 (2.38)	9.2 (1.9)		9.85 (2.13)	
Refinement						
	Model R / R_{free}-factor (%) [c]	19.3 / 25.7	16.3 / 21.6		20.2 / 25.5	
	No. of molecules in a.u.	12	12		12	
	Ligand occupancy and B-factor ($Å^2$)		Occupancy	B-factor	Occupancy	B-factor
	HG [d]		0.89 (12)	18.3 (12)	0.83 (8)	18.5 (8)
	MAA chain A [e]				0.85 (1)	21.4 (1)
	HMO chain C [e]				0.80 (1)	16.0 (1)
	AKY chain F [e]				0.80 (1)	17.7 (1)
	AKY chain L [e]				0.60 (1)	17.9 (1)
	Rms deviation from ideal geometry					
	Bonds (Å)	0.010	0.009		0.010	
	Angles (°)	1.089	1.109		1.160	
	Ramachandran statistics (%)					
	Allowed	97.0	97.7		99.4	
	Outliers	0.1	0.0		0.08	

Numbers in brackets denote the values found in the highest resolution shell.

[a] $R_s = \Sigma_h \Sigma_i |I_i(h) - \langle I(h) \rangle| / \Sigma_h \Sigma_i I_i(h)$; where i are the independent observations of reflection h.

[b] Multiplicity-independent merging *R* factor ($R_{r.i.m.}$) and precision-indicating merging *R* factor ($R_{p.i.m.}$) (3).

[c] The R_{free} factor was calculated from 5% of the data, which were removed at random before the refinement was carried out.

[d] Occupancies and B-factors of ligands are average value calculated from numbers of molecules possessing the same ligand in a.u. (brackets). Iron-bound solvent molecules are not included.

[e] MAA, ring-open product; AKY, alkylperoxo species; HMO, superoxo:semiquinone intermediate.

Table S2. Selected bond lengths of ferrous ion coordination in Fe^{2+}-only and Fe^{2+}:HG. Average bond lengths with standard deviation of all 12 refined molecules in the asymmetric unit are shown in Angstrom.

	Fe^{2+}-only	**Fe^{2+}:HG**
Fe–W1-O	2.15 ± 0.06	
Fe–W2-O	2.20 ± 0.05	2.19 ± 0.04
Fe–E337-Oε1	2.31 ± 0.06	2.32 ± 0.03
Fe–E337-Oε2	2.17 ± 0.08	2.11 ± 0.05
Fe–H367-Nε2	2.21 ± 0.08	2.15 ± 0.04
Fe–H331-Nδ1	2.21 ± 0.09	2.17 ± 0.05
Fe–HG-O1		1.98 ± 0.10

Table S3. Occupancies and B-factors of ligands from structures of the ring-open product (chain A), superoxo:semiquinone (chain C) and the alkylperoxo-intermediate (chain F and L). Averaged values are reported in Tab. S1. Atoms are numbered as indicated.

Atom	**Ring-open product**		**Superoxo:semiquinone**		**Alkylperoxo-intermediate**	
	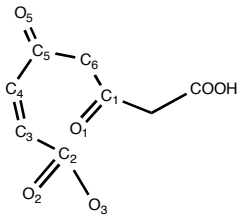		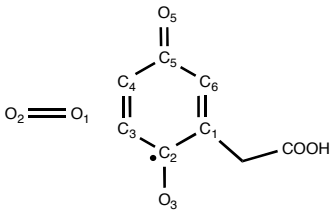		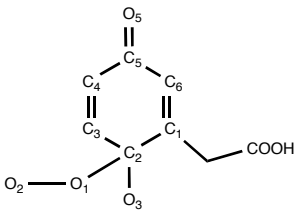	
	Occupancy	B-factor (Å^2)	Occupancy	B-factor (Å^2)	Occupancy	B-factor (Å^2)
Fe^{2+}	1.00	11.1	1.00	10.3	1.00 (F), 1.00 (L)	12.0 (F), 13.2 (L)
O1	0.85	18.0	0.80	13.0	0.80 (F), 0.60 (L)	13.0 (F), 19.2 (L)
O2	0.85	19.0	0.80	11.5	0.80 (F), 0.60 (L)	18.2 (F), 17.5 (L)
C1	0.85	25.9	0.80	18.6	0.80 (F), 0.60 (L)	16.1 (F), 19.2 (L)
C2	0.85	18.6	0.80	17.0	0.80 (F), 0.60 (L)	16.6 (F), 16.7 (L)
C3	0.85	20.3	0.80	16.7	0.80 (F), 0.60 (L)	17.9 (F), 17.6 (L)
C4	0.85	18.1	0.80	19.3	0.80 (F), 0.60 (L)	23.1 (F), 20.1 (L)
C5	0.85	21.3	0.80	18.2	0.80 (F), 0.60 (L)	20.1 (F), 18.5 (L)
C6	0.85	23.3	0.80	17.1	0.80 (F), 0.60 (L)	18.7 (F), 18.3 (L)
O3	0.85	30.0	0.80	10.2	0.80 (F), 0.60 (L)	13.1 (F), 11.6 (L)
O5	0.85	19.2	0.80	18.4	0.80 (F), 0.60 (L)	20.4 (F), 20.1 (L)

SUPPORTING FIGURES

Figure S1. (a) Superposition of the crystal structures of HGDOs from *P. putida* ($HGDO_{Pp}$) and man ($HGDO_{Hs}$), shown looking along the two-fold axis that creates the dimer of trimers (side view). The hexamer of $HGDO_{Pp}$ is colored in *cyan*, *green*, *pink*, *orange*, *yellow* and *blue* and is superposed with $HGDO_{Hs}$, which is colored *gray* (rmsd for C^{α} atoms of 1.8 Å). (b) Comparison of the active sites of the two HGDOs, focusing on the Fe^{2+} coordination by the facial triad motif. A dotted-circle indicates the difference between monodentate ($HGDO_{Hs}$) and bidentate ($HGDO_{Pp}$) coordination of Fe^{2+} by glutamate. The iron atoms are shown as spheres. (c) Surface representation of $HGDO_{Pp}$. Active site of Fe^{2+}-bound $HGDO_{Pp}$ with the iron atom shown in *purple*. The active site lid is disordered and not observed in the electron density map. (d) Appearance of the active site lid consisting of residues Gly344–Glu351 upon HG binding in the Fe^{2+}:HG structure. Binding of HG to the Fe^{2+} decreases the conformational flexibility of the active site lid by recruiting Tyr346 to bind HG.

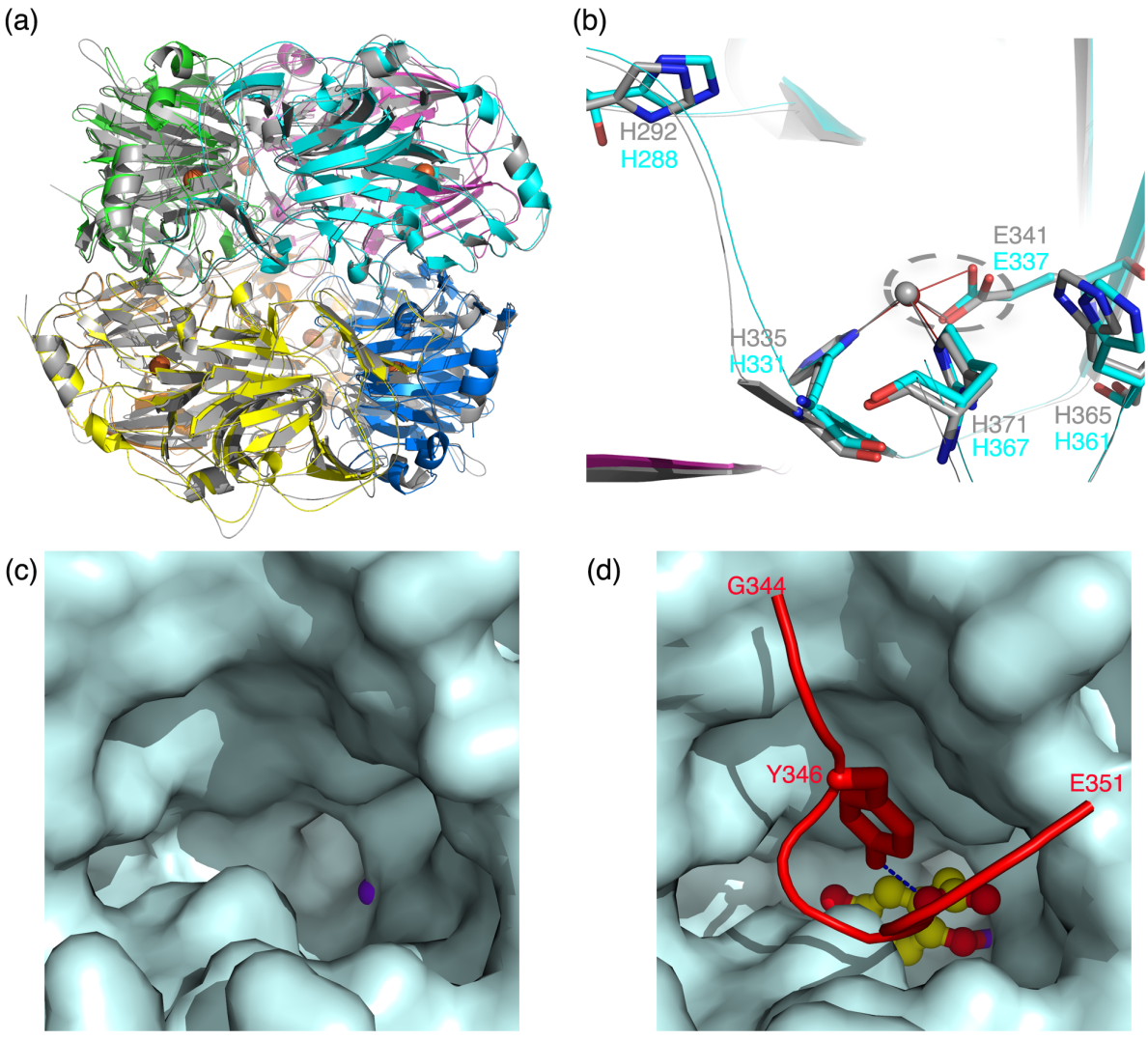

Figure S2. Detailed view of the active site structures of $HGDO_{Pp}$ in the resting state (Fe^{2+}-only) and in complex with HG (Fe^{2+}:HG). Dashed lines show putative hydrogen bonds (Å) and purple solid lines bonds between iron and its ligands (Å). (a) Fe^{2+}-only active site environment. Hydrophobic residues are indicated by surface presentation with F52* originating from an adjacent subunit. (b) Structure of Fe^{2+}:HG.

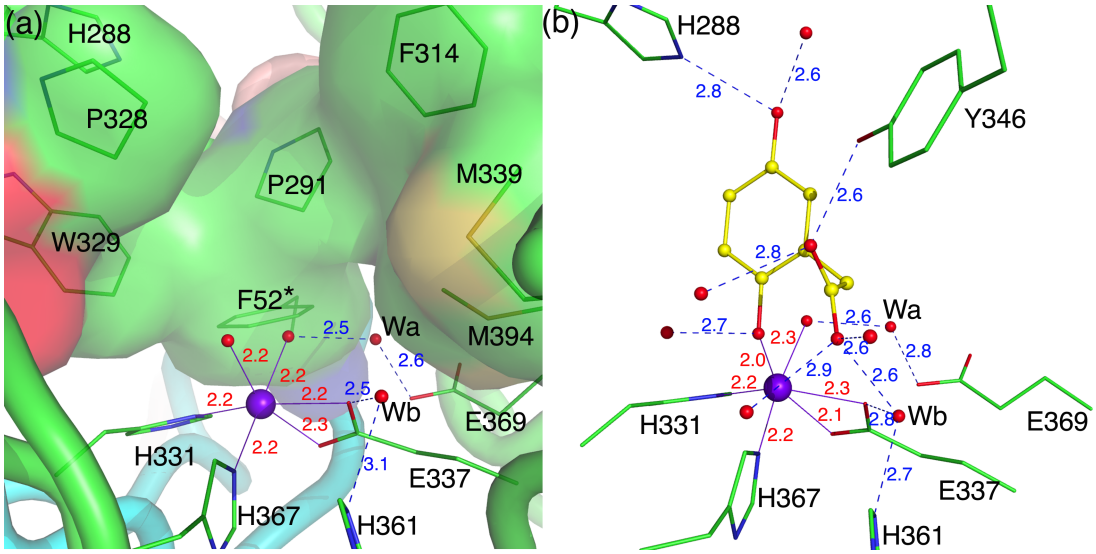

Figure S3. Omit and control electron densities for the superoxo:semiquinone state in chain C.
(a) Dioxygen omitted: Initial refinement using the Fe^{2+}:HG model lacking Fe^{2+} coordinating water/dioxygen molecules. The final dioxygen model (transparent stick) is shown for clarity and to illustrate the diatomic electron density. (b) Control model with a water instead of dioxygen and superoxo-semiquinone in place of HG-semiquinone.
Weighted $2F_{obs} - F_{calc}$ maps (blue mesh) are contoured at 1.0 σ (a) and 1.2 σ (b). $F_{obs} - F_{calc}$ omit maps (green mesh) generated by several restrained refinement cycles are contoured at 3.0 σ (a) and 3.2 σ (b). Atoms are colored gray for iron, green for carbon and red for oxygen.

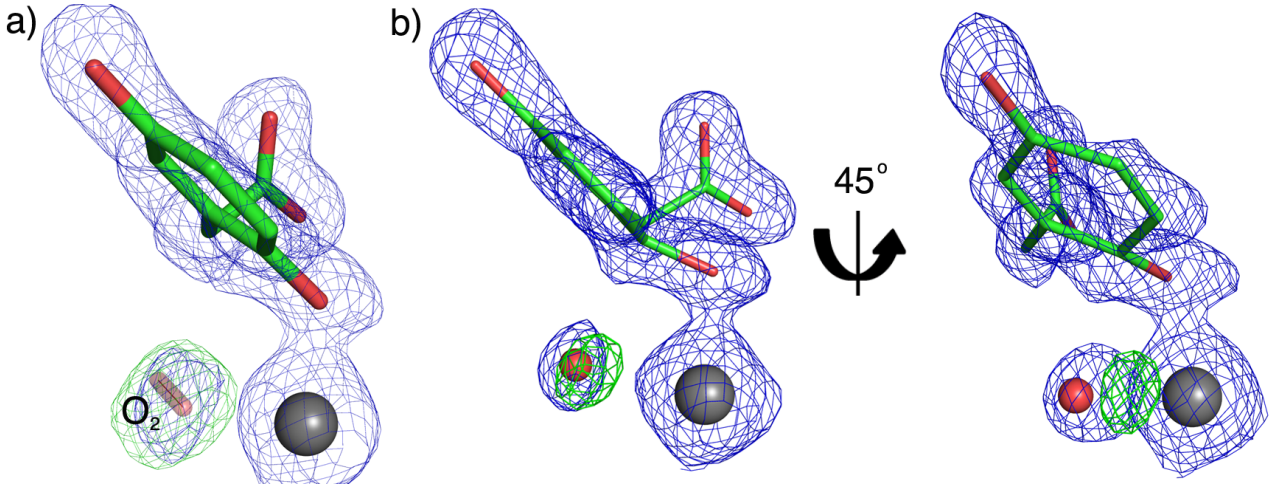

Figure S4. Omit and control electron densities for the alkylperoxo states in chain F (a and b) and L (c and d).

(a/c) Oxygen omitted: Electron density observed after initial refinement against the Fe^{2+}:HG model without other Fe^{2+} ligands are shown for chains F and chain L, respectively. (b/d) Superoxo:semiquinone control model for the alkylperoxo states in chains F and L. The final alkylperoxo model is shown as thin lines with yellow-colored carbon.

Weighted $2F_{obs} - F_{calc}$ maps (blue mesh) are contoured at 1.0 σ (a - d). $F_{obs} - F_{calc}$ omit maps (green mesh) generated after several cycles of restrained refinement are contoured at 3.2 σ (a - d). Atoms are colored gray for iron, green for carbon and red for oxygen.

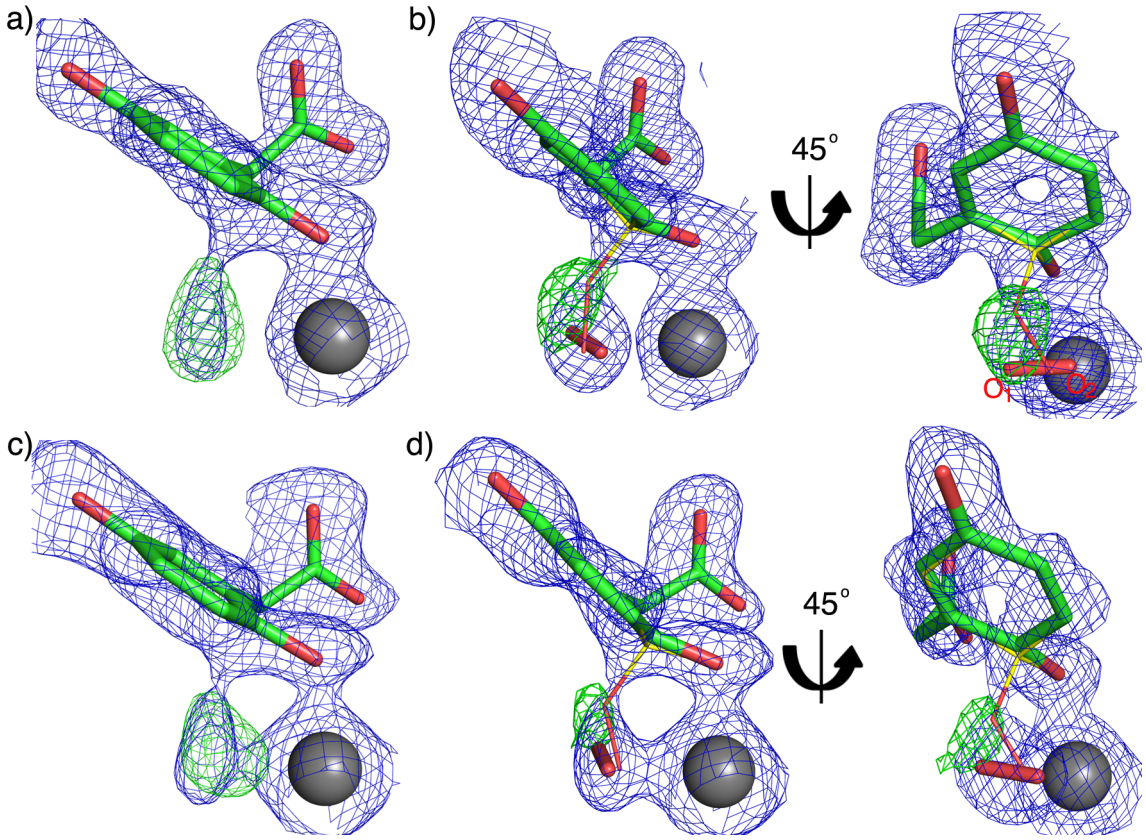

Figure S5. Second coordination sphere of the superoxo:semiquinone intermediate (a) and alkylperoxo-intermediate (b) structures. Possible hydrogen bonding interaction networks mediated by solvent molecules are indicated by dashed-lines (Å). Solvent molecules Wa and Wb are labeled. Ligand atoms are colored red for oxygen, purple for iron, orange for carbon, where carbon atoms from residues interacting via water molecules with the intermediates are colored yellow.

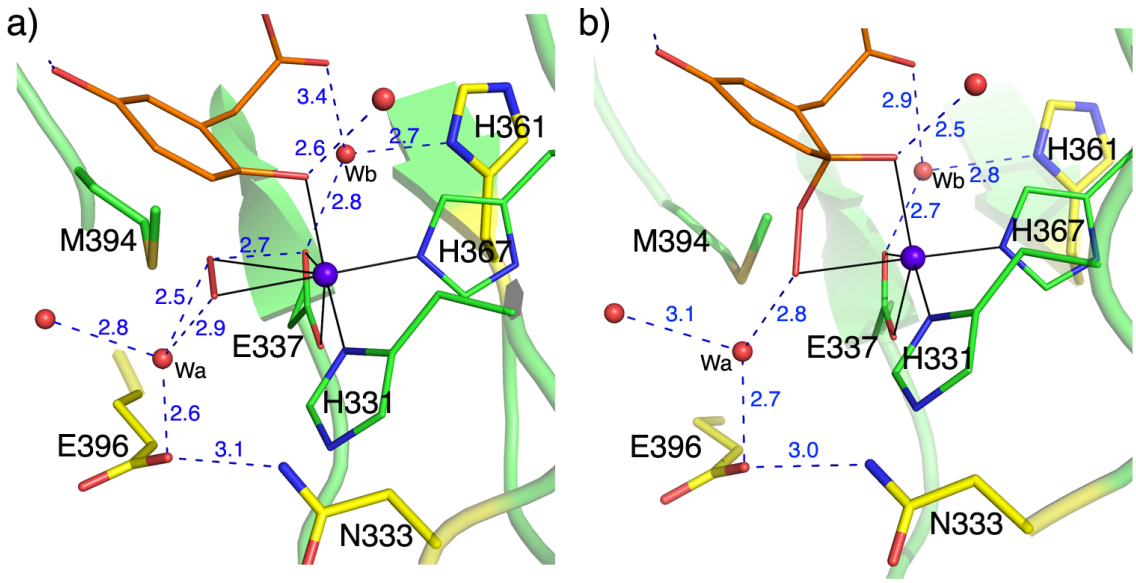

Figure S6. Molecular channels in the HG-bound structure (Fe^{2+}:HG) calculated using HOLLOW (4). Surface of the interior cavity of the hexamer shown along the threefold axis (a) and side view (b). Arrows indicate a possible path for O_2 from the surface running along the threefold axis to the central cavity generated by the twofold axis. (c) Enlarged view of the dotted-square box in (b), showing the branch leading to the vacant coordination site of the Fe^{2+} ion occupied by water molecule W2, where the binding site of dioxygen was detected.

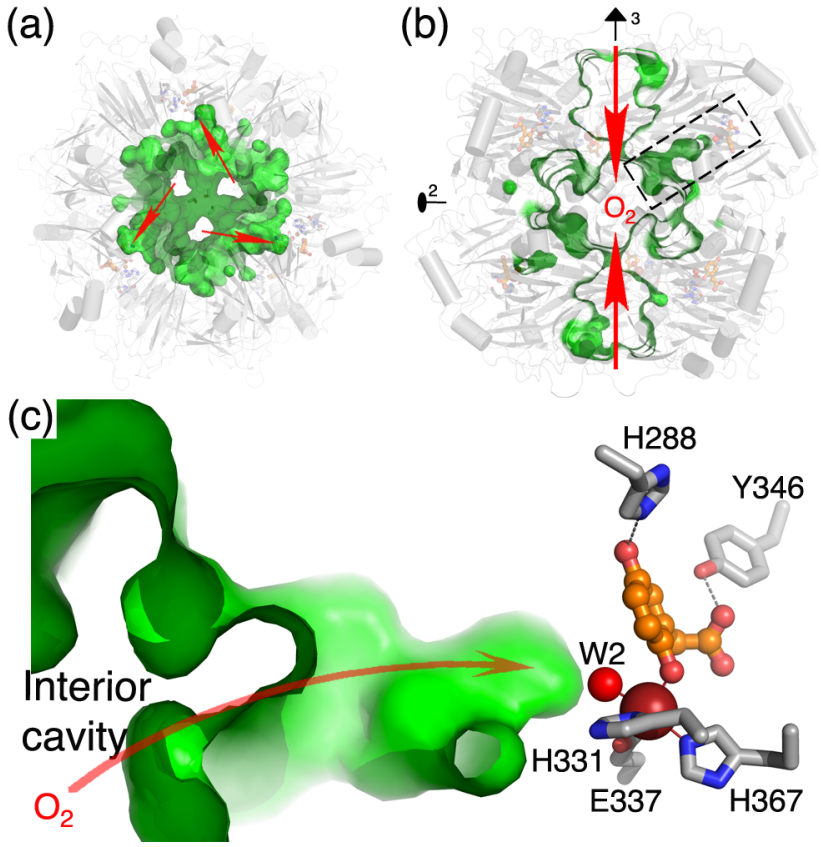

Figure S7. Superposition of the observed reaction intermediates in stereo presentation: Fe^{2+}-only (orange), Fe^{2+}:HG (cyan), O_2:HG (magenta), alkylperoxo-intermediate (green) and product-bound (yellow). Two solvent molecules observed in the Fe^{2+}-only structure are shown as orange spheres. A cavity below the O2 atom of the bound dioxygen is pointing towards the central cavity shown in Fig. S6. The rmsd values of Cα atoms of all superposed structures are smaller than 0.2 Å. Three critical spots to hold the substrate and intermediates in the active site are marked as transparent cyan spheres.

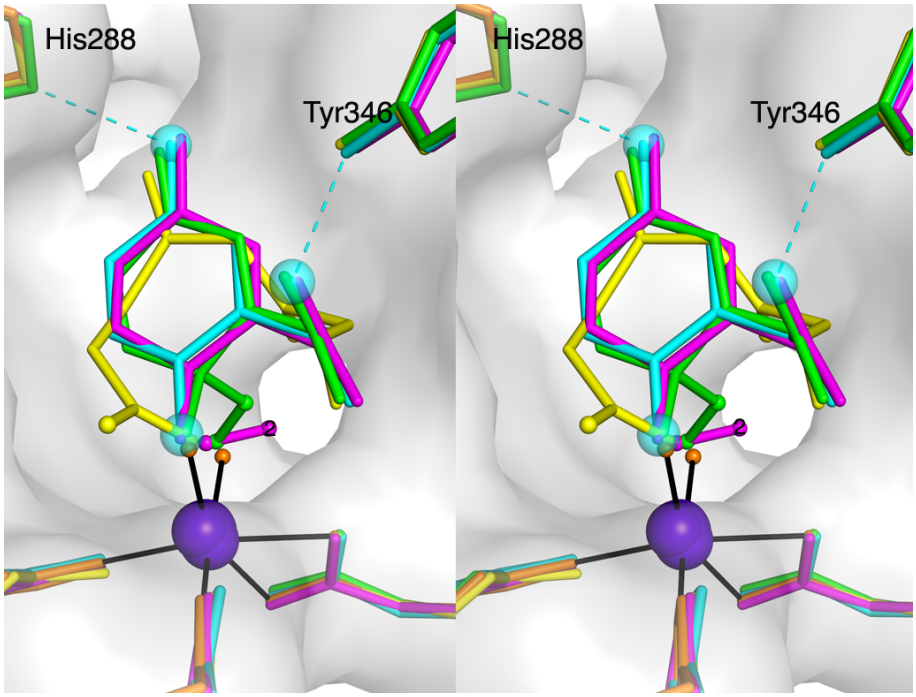

Figure S8. Crystal packing analysis. (a) Crystal packing of the Fe^{2+}:HG-O_2 structure. The central black rectangle shows the two hexamers of $HGDO_{Pp}$ in the asymmetric unit (equivalent with the unit cell in space group *P*1), surrounded by symmetry mates. HG-bound subunits are colored yellow. Residues of different subunits closer than 5 Å from each other were defined as possible crystal contacts and are shown as red sticks. A close-up view of the crystal contacts between different chains are shown in the four black-lined boxes. The active site lid (G344-E351) is highlighted in blue. (b) Schematic depiction of the twelve subunits of the asymmetric unit. Chain C (superoxo:HG-semiquinone intermediate), F and L (alkylperoxo intermediate), and chain A (product after ring-cleavage) are colored as violet, purple and green, and cyan, respectively.

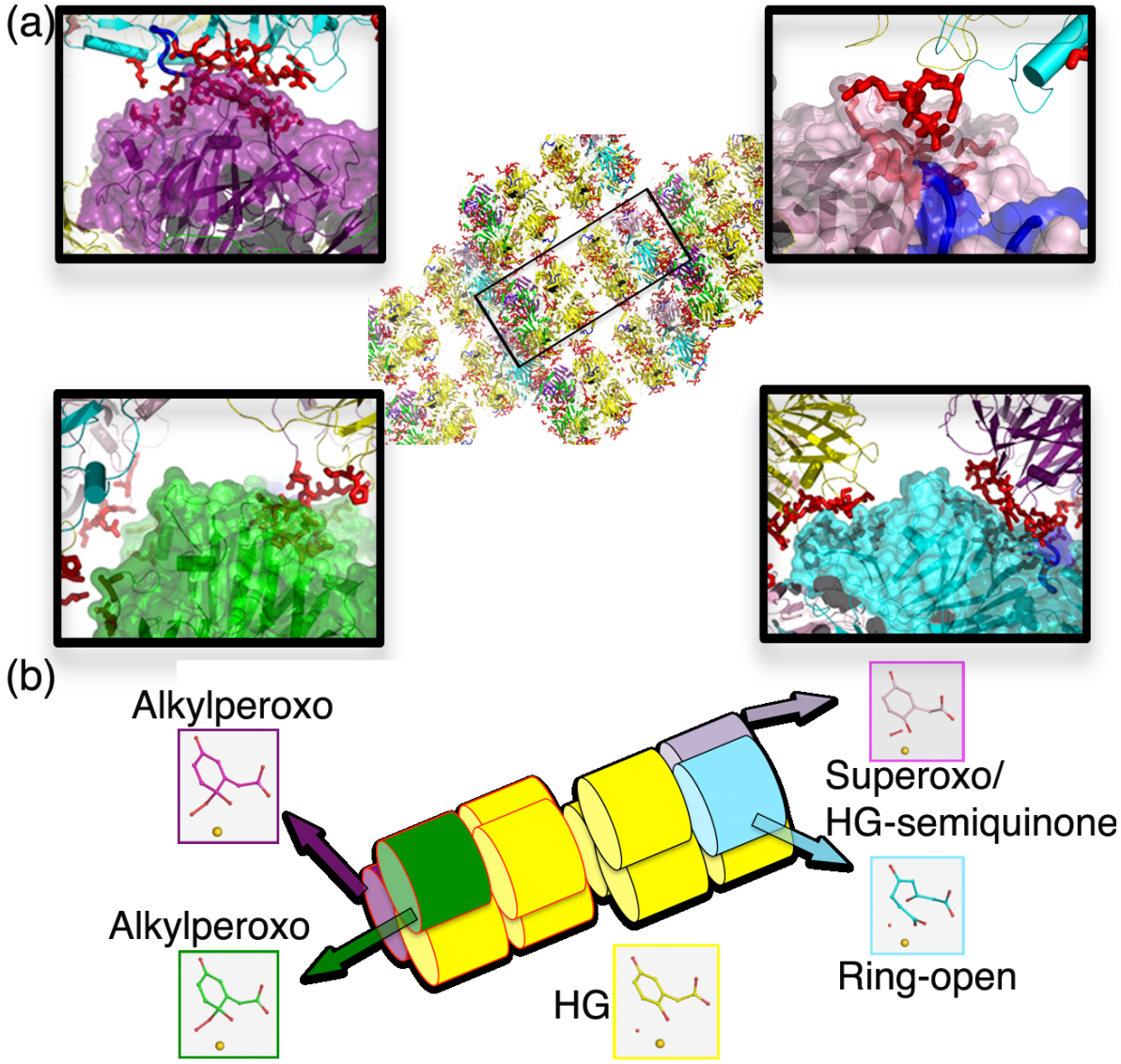

Figure S9. Proposed reaction mechanism for the oxidative aromatic ring-cleavage of HG by HGDO. Reaction intermediates (I) to (V) are based on the active site structures reported in this study (Fig. 3). Three unobserved, possibly short-lived intermediates are drawn in square brackets. The putative formation of a seven-member lactone (Int^3) via a gem-diol (Int^1) and epoxide (Int^2) intermediate is based on mechanistic similarity of HGDO to 2,3-HPCD as described in the text.